Available online at www.elixirpublishers.com (Elixir International Journal)

Computational Physics

Elixir Computational Physics 92 (2016) 38706-38717

ISSN: 2229-712X

Molecular structure, Vibrational spectra, non-linear optical properties, and docking study of 2-Methylidene -4-oxo-4-[(2, 4, 5-trichlorophenyl) amino]butanoic acid

K. Vanasundari[1], V. Balachandran[1], M. Kavimani[1] and B. Narayana[2]

[1]Department of Physics, Arignar Anna Government Arts College, Musiri, Tiruchirappalli - 621 211, India.

[2]Department of Studies in Chemistry, Mangalore University, Mangalagangotri - 574 199, India.

ARTICLE INFO

Article history:

Received: 7 February 2017;

Received in revised form:

5 March 2017;

Accepted: 16 March 2017;

Keywords

FT-IR,

FT-Raman,

NMR,

HOMO-LUMO,

Fukui functions,

Docking studies.

ABSTRACT

In this work, the Fourier transform Raman and Fourier transform infrared spectra of 2-Methylidene -4-oxo-4-[(2, 4, 5-trichlorophenyl) amino] butanoic acid were recorded. The structural and spectroscopic analyses of the above compound were made by using B3LYP/ DGDZVP2 and DGTZVP basis sets. The detailed interpretation of the vibrational spectra has been carried out with the aid of VEDA program. The observed and calculated frequencies are found to be in good agreement. NMR spectra have been recorded and analysed. To investigate microscopic second order nonlinear optical behavior of the title compound, the electric dipole moment μ, the polarizability α and hyper polarizability β were computed. According to our calculation, the title compound exhibiting non-zero β total value revealing microscopic second order NLO behavior. The value of HOMO-LUMO, Mulliken and natural charges have been calculated and analyzed. The natural bond orbital analysis confirms the occurrences of intra-molecular charge transfer interaction. Electrostatic potential surface has been plotted for predicting the structural activity relationship. Global reactivity descriptors and Fukui functions have been calculated for predicting the chemical reactivity and the stability of the chemical system. To test the biological activity of the title compound docking studies have been carried out.

1. Introduction

Butyric acid also known under the systematic name butanoic acid is a carboxylic acid occurring in the form of esters and animal fats and plant oils. I t is found in milk especially goat, sheep, buffalo milk, butter a nd cheese. It has an unpleasant smell and acrid taste, with a sweetish after taste similar to ether. Butyrate helps to protect colonic mucosa from oxidative stress and inhibits its inflammation while promoting satiety [1]. In chemical industries, the main application of butyric acid is the manufacture of cellulose acetate butyrate plastics [2]. By introducing the butyryl group into cellulose acetate polymers, the resulting polymer exhibits better performance in terms of its solubility in organic solvents due to enhanced hydrophobicity, better flexibility, and light and cold resistance . A recent study also showed the possibility of mixing cellulose acetate butyrate (CAB) with another polymer, poly (3-hydroxybutyrate) (PHB), which can also be prepared from butyric acid [3], to decrease the production cost of PHB and improve its characteristics [4]. Furthermore, although butyric acid itself has an unpleasant odor, butyric acid esters such as methyl, ethyl and amyl butyrate are used as fragrant and flavoring agents in beverages, foods and cosmetic industries [5, 6].

Literature survey reveals that no experimental and theoretical vibrational analysis for [2-Methylidene -4-oxo-4-[(2, 4, 5-trichlorophenyl) amino] Butanoic acid (MTA) molecule has been performed yet.

A systematic study on the molecular structure and vibrational spectra helps in understanding the properties of the molecule in depth. Vibrational spectroscopy is an analytical tool for providing information about structure, composition, conformation and intermolecular interactions of complex molecules [7, 8]. The present work describes the vibrational spectral investigations of MTA aided by density functional computations to elucidate the correlation between the molecular structure and biological activity. The redistribution of electron density in various bonding and antibonding orbitals along with stabilization energies have been calculated by natural bond orbital analysis to give clear proof of stabilization originating from hyper-conjugation of a variety of intra-molecular interaction.

NMR spectra were also reported both experimentally and theoretically. The nonlinear properties, Mulliken atomic charg es and Fukui functions have been analyzed. Molecular docking is a powerful computational tool in predicting the binding affinity of a ligand with the proteins, which are very much useful and effective in modern structure-based drug designing. The structure of the target protein can be obtained from the protein data bank (PDB) format. The ligand protein molecular docking can predict that the preferred orientation of the ligand with respect to the protein to form a stable complex and its derivatives.

Tele: +91 9894253672

E-mail address: brsbala@rediffmail.com

2. Experimental and computational details

The FT-IR spectrum was recorded in the region 4000-450 cm^{-1} on Perkin Elmer spectrometer equipped with MCTdetector using KBr beam splitter. The FT-Raman spectrum was also recorded using 1064 nm line of Nd:YAG laser as excitation wavelength in the region 4000-50 cm^{-1} BRUKER RFS 27 FT-Raman Spectrometer. NMR spectra are performed in BRUKER AV500 MHz at 300 K. ^{1}H and ^{13}C NMR spectra are obtained at a base frequency of 600-150 MHz. The entire quantum chemical calculations have performed at DFT/B3LYP with DGDZVP2 and DGTZVP basis sets using the Gaussian 09W program package [9]. The optimized structural parameters have been evaluated for the calculation of vibrational frequencies at Becke's three parameter hybrid model using the Lee–Yang–Parr [10, 11] correlation functional (B3LYP) method. The assignments of the calculated normal modes have been made on the basis of the corresponding PEDs. These calculations were done with the VEDA 4.0 program written by Jamroz [12]. Gauss view program [13] has been considered to get visual animation and also for the verification of the normal modes assignment. The natural bonding orbital's (NBO) calculations were performed using NBO program as implemented in Gaussian 09 Package.

3. Results and Discussion

3.1 Molecular geometry

The geometry of the molecule under investigation is considered by possessing C_1 point group symmetry. The optimized molecular structure of MTA along with numbering of atom is shown in Fig. 1. To understand the vibrational frequencies, it is essential to know the geometry of the compound. The values of the optimized bond lengths, bond angles, and dihedral angles of MTA are presented in Table 1. Generally, the carbon-carbon bonds in phenyl ring are not the same length. The bonds C_1-C_2, C_2-C_3, C_3-C_4, C_4-C_5, and C_5-C_6 are varied. The C-C bond lengths of MTA are fall in the range 1.37-1.57Å which is in good agreement with the reported values [14]. The calculated shorter bond length is O_{25}-H_{26} =0.96 Å and

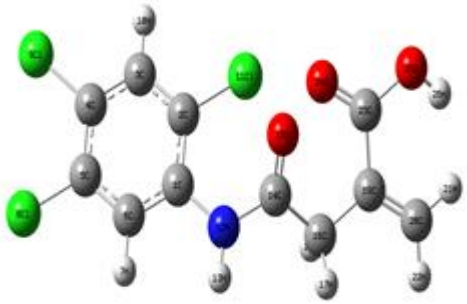

Fig 1.Optimized geometry of 2-Methylidene -4-oxo-4-[(2, 4, 5-trichlorophenyl) amino] Butanoic acid.

longer bond length is Cl_{11}-O_{24}=2.074Å. Ergodu et al. [15] reported that the optimized bond angles of C-C-C and C-N-C in phenyl ring fall in the range from 119°-120°. In the present case, these angles fall in the range 118°-122°. For MTA, the shorter and longer bond angles are C_2-Cl_{11}-O_{15} =101.34°; Cl_{11}-C_{23}-C_{24}=147.61°. The greater bond angles are assigned to be due to the delocalization of electrons due to the presence of phenyl ring.

3.2 Vibrational spectral analysis

The vibrational spectral analysis of MTA is performed on the basis of the characteristic vibrations of several functional groups such as amino group, methyl group, and carboxyl group and phenyl ring modes. The computed wavenumbers and their vibrational assignments are listed in Table 2. For visual comparison, the observed FT-IR and Raman spectra are presented in Figs. 2 and 3, respectively.

From the structural point of view, the MTA is assumed to have C_1 point group symmetry. It consists of 26 atoms, so it has 72 fundamental vibrational modes.

The C-H ring stretching vibrations occurs in the region 3100-3000 cm^{-1} which is the characteristic region of the ready identification of the C-H stretching vibrations. In this region, the bands are not affected appreciably by the nature of the substituent. Strong bands appeared at 3014 cm^{-1} in FT-IR spectrum and at 3020 cm^{-1} FT-Raman spectrum are assigned to C-H ring stretching vibrations. As evident from the PED column they are pure stretching vibrations almost contributing to above 98%. Guidara et al. [16] reported that the in-plane and out-of-plane aromatic C-H bending vibrations occur in the range 1300-1000 cm^{-1} and 1000-750 cm^{-1}. In case of MTA, C-H in-plane bending is observed experimentally at 1183, 1141, 1131 and 1078 cm^{-1}. The medium strong, weak bands that arise at 966, 900, 875, and 820 cm^{-1} in the Raman spectrum are assigned to the C-H out-of-plane bending. In the present case, the C-H in plane bending vibrations of MTA is computed in the range 1497-1131 cm^{-1} DGDZVP2 method and the range1545-1262 cm^{-1} by DGTZVP method. In the present study, the phenyl ring possesses six ring carbon-carbon stretching vibrations in the region 1070-1150 cm^{-1}. As revealed by PED, the ring C-C stretching modes are observed at 1629, 1595, 1587 and 1510 cm^{-1} in FT-IR. In MTA, ring in-plane and out-of-plane bending modes are observed at 543, and 624 cm^{-1} in FT-IR spectrum 525 and 625 cm^{-1} in FT-Raman spectrum. The C-Cl absorption is observed in the broad region between 834 and 561 cm^{-1}. Thus, the strong bands in IR at 834, 821 and 672 cm^{-1} are assigned to the C-Cl stretching modes of MTA. This assignment is well agreement with the literature of 2-amino-5-chlorobenzoxazole [17].

For the assignment of CH_2 group frequencies, basically six fundamentals can be associated to each CH_2 group namely, CH_2 symmetric stretching, CH_2 asymmetric stretching, CH_2 rocking, and CH_2 scissoring modes belongs to in-plane vibrations, CH_2 wagging, and CH_2 twisting deformation of CH_2 group would be expected to be for out-of-plane modes.

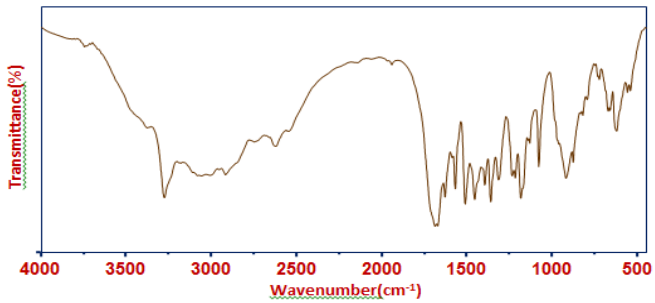

Fig 2.Observed FT-I R spectrum of 2-Methylidene -4-oxo-4-[(2, 4, 5-trichlorophenyl) amino] Butanoic acid.

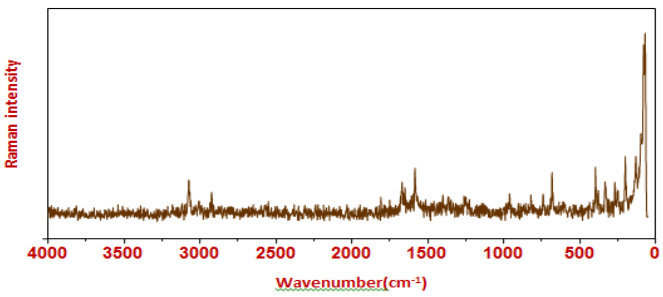

Fig 3. Observed FT-Raman spectrum of 2-Methylidene -4-oxo-4-[(2, 4, 5-trichlorophenyl) amino] Butanoic acid.

Table 1. Optimized geometrical parameters of 2-Methylidene -4-oxo-4-[(2, 4, 5-trichlorophenyl) amino] Butanoic acid.

Bond length(Å)			Bond angle(deg)			Dihedral angle(deg)		
Parameters	B3LYP/ DGDZVP2	B3LYP/ DGTZVP	Parameters	B3LYP/ DGDZVP 2	B3LYP/ DGTZVP	Parameters	B3LYP/ DGDZV P2	B3LYP/ DGTZVP
C_1-C_2	1.40	1.40	C_2-C_1-C_6	119.99	118.29	C_6-C_1-C_2-C_3	0.03	0.45
C_1-C_6	1.39	1.40	C_2-C_1-N $_{12}$	119.98	118.93	C_6-C_1-C_2-Cl_{11}	-179.98	-179.40
C_1-N_{12}	1.47	1.33	C_6-C_1-N_{12}	120.02	122.78	N_{12}-C_1-C_2-C_3	-180.00	-179.75
C_2-C_3	1.39	1.34	C_1-C_2-C_3	119.99	120.53	N_{12}-C_1-C_2-Cl_{11}	-0.02	0.39
C2-C_{11}	1.76	1.72	C_1-C_2-Cl_{11}	119.99	119.18	C_2-C_1-C_6-C_5	0.01	-0.26
C_3-C_4	1.40	1.38	C_3-C_2-Cl_{11}	120.01	120.29	C_2-C_1-C_6-H_7	-180.00	179.50
C_3-Cl_{10}	1.07	1.07	C_2-C_3-C_4	120.01	121.01	N_{12}-C_1-C_6-C_5	-179.96	179.96
C_4-C_5	1.39	1.40	C_2-C_3-Cl_{10}	120.01	120.95	N_{12}-C_1-C_6-H_7	0.03	-0.28
C_4-H_9	1.76	1.07	C_4-C_3-Cl_{10}	119.98	118.04	C_2-C_1-N_{12}-H_{13}	-179.95	7.14
C_5-C_6	1.40	1.39	C_3-C_4-C_5	120.00	118.60	C_2-C_1-N_{12}-C_{14}	0.05	-175.88
C_5-H_8	1.76	1.76	C_3-C_4-H_9	120.00	119.91	C_6-C_1-N_{12}-H_{13}	0.02	-173.08
C_6-H_7	1.10	1.40	C_5-C_4-H_9	120.00	121.49	C_6-C_1-N_{12}-C_{14}	-179.98	3.90
Cl11-O_{15}	1.91	1.76	C_4-C_5-C_6	120.00	121.32	C_1-C_2-C_3-C_4	-0.06	-0.33
Cl_{11}-O_{24}	2.07	1.10	C_4-C_5-H_8	120.01	119.41	C_1-C_2-C_3-Cl_{10}	-179.98	179.81
N_{12}-H_{13}	1.00	1.01	C_6-C_5-H_8	119.99	119.27	Cl_{11}-C_2-C_3-C_4	179.96	179.53
N_{12}-C_{14}	1.47	2.07	C_1-C_6-C_5	120.00	120.25	Cl_{11}-C_2-C_3-Cl_{10}	0.04	-0.34
C_{14}-O_{15}	1.26	1.12	C_1-C_6-H_7	120.01	118.69	C_1-C_2-Cl_{11}-O_{15}	-24.29	1.85
C_{14}-C_{16}	1.54	1.47	C_5-C_6-H_7	119.98	121.06	C_1-C_2-Cl_{11}-O_{24}	-18.00	-18.75
O_{15}-O_{24}	1.57	1.26	C_2-Cl_{11}-O_{15}	101.34	49.43	C_3-C_2-Cl_{11}-O_{15}	155.69	-178.00
C_{16}-C_{17}	1.07	1.54	C_2-Cl_{11}-O_{24}	147.23	104.34	C_3-C_2-Cl_{11}-O_{24}	161.98	161.40
C_{16}-H_{18}	1.07	1.07	C_1-N_{12}-H_{13}	120.00	116.94	C_2-C_3-C_4-C_5	0.03	0.00
C_{16}-C_{19}	1.54	1.57	C_1-N_{12}-C_{14}	120.00	117.24	C_2-C_3-C_4-H_9	-179.97	-179.94
C_{19}-C_{20}	1.36	1.54	H_{13}-N_{12}-C_{14}	120.00	115.75	Cl_{10}-C_3-C_4-C_5	179.95	179.87
C_{19}-C_{23}	1.54	1.36	N_{12}-$C1_4$-O_{15}	120.00	125.10	Cl_{10}-C_3-C_4-H_9	-0.05	-0.07
C_{20}-H_{21}	1.07	1.54	N_{12}-C_{14}-C_{16}	120.00	114.93	C_3-C_4-C_5-C_6	0.01	0.20
C_{20}-H_{22}	1.07	1.07	O_{15}-C_{14}-C_{16}	120.00	119.96	C_3-C_4-C_5-H_8	179.99	-179.88
C_{23}-O_{24}	1.26	1.07	Cl_{11}-O_{15}-C_{14}	101.63	35.18	H_9-C_4-C_5-C_6	-179.98	-179.86
C_{23}-O_{25}	1.43	1.22	C_{14}-O_{15}-O_{24}	121.31	13.21	H_9-C_4-C_5-H_8	-0.01	0.06
O_{25}-H_{26}	0.96	0.98	C_{14}-C_{16}-H_{17}	109.47	105.45	C_4-C_5-C_6-C_1	-0.04	-0.07
			C_{14}-C_{16}-H_{18}	109.47	109.92	C_4-C_5-C_6-H_7	179.98	-179.82
			C_{14}-C_{16}-C_{19}	109.47	112.68	H_8-C_5-C_6-C_1	179.99	-179.99
			H_{17}-C_{16}-H_{18}	109.47	108.90	H_8-C_5-C_6-H_7	0.00	0.26
			H_{17}-C_{16}-C_{19}	109.47	109.61	C_2-Cl_{11}-O_{15}-C_{14}	55.86	-175.91
			H_{18}-C_{16}-C_{19}	109.47	110.12	C_2-Cl_{11}-O_{24}-C_{23}	76.45	-19.89
			C_{16}-C_{19}-C_{20}	120.23	122.74	C_1-N_{12}-C_{14}-O_{15}	45.00	-1.71
			C_{16}-C_{19}-C_{23}	119.89	114.86	C_1-N_{12}-C_{14}-C_{16}	-135.00	178.16
			C_{20}-C_{19}-C_{23}	119.89	122.26	H_{13}-N_{12}-C_{14}-O_{15}	-135.00	175.30
			C_{19}-C_{20}-H_{21}	120.00	123.37	H_{13}-N_{12}-C_{14}-C_{16}	45.00	-4.83
			C_{19}-C_{20}-H_{22}	120.00	120.69	N_{12}-C_{14}-O_{15}-Cl_{11}	-69.48	3.51
			H_{21}-C_{20}-H_{22}	120.00	115.87	N_{12}-C_{14}-O_{15}-O_{24}	-145.75	-103.37
			C_{19}-C_{23}-O_{24}	120.23	122.11	C_{16}-C_{14}-O_{15}-Cl_{11}	110.52	-176.35
			C_{19}-C_{23}-O_{25}	119.89	118.46	C_{16}-C_{14}-O_{15}-O_{24}	34.25	76.77
			O_{24}-C_{23}-O_{25}	119.89	119.43	N_{12}-C_{14}-C_{16}-H_{17}	-60.25	-162.54
			Cl_{11}-C_{23}-C_{24}	147.62	151.54	N_{12}-C_{14}-C_{16}-H_{18}	59.75	-45.31
			O_{15}-C_{23}-C_{24}	111.21	76.47	N_{12}-C_{14}-C_{16}-C_{19}	179.75	77.92
			C_{23}-O_{25}-H_{26}	109.47	113.79	O_{15}-C_{14}-C_{16}-H_{17}	119.75	17.33
						O_{15}-C_{14}-C_{16}-H_{18}	-120.25	134.57
						O_{15}-C_{14}-C_{16}-C_{19}	-0.25	-102.20
						C_{14}-O_{15}-O_{24}-C_{23}	-52.00	-140.04
						C_{14}-C_{16}-C_{19}-C_{20}	162.13	85.66
						C_{14}-C_{16}-C_{19}-C_{23}	-17.87	-90.14
						H_{17}-C_{16}-C_{19}-C_{20}	42.13	-31.43
						H_{17}-C_{16}-C_{19}-C_{23}	-137.87	152.77
						H_{18}-C_{16}-C_{19}-C_{20}	-77.87	-151.21
						H_{18}-C_{16}-C_{19}-C_{23}	102.13	32.99
						C_{16}-C_{19}-C_{20}-H_{21}	176.06	-175.03

						C_{16}-C_{19}-C_{20}-H_{22}	-3.94	2.05
						C_{23}-C_{19}-C_{20}-H_{21}	-3.94	0.46
						C_{23}-C_{19}-C_{20}-C_{23}	176.06	177.55
						C_{16}-C_{19}-C_{23}-O_{24}	0.00	20.28
						C_{16}-C_{19}-C_{23}-O_{25}	180.00	-159.41
						C_{20}-C_{19}-C_{23}-O_{25}	180.00	-155.54
						C_{20}-C_{19}-C_{23}-O_{25}	0.00	24.77
						C_{19}-C_{23}-O_{24}-Cl_{11}	-39.40	53.81
						C_{19}-C_{23}-O_{24}-O_{15}	30.54	14.85
						O_{25}-C_{23}-O_{24}-Cl_{11}	140.60	-126.50
						O_{25}-C_{23}-O_{24}-O_{15}	-149.46	-165.47
						C_{19}-C_{23}-O_{25}-H_{26}	16.63	10.06
						O_{24}-C_{23}-O_{25}-H_{26}	-163.37	-169.64

Table 2. Observed IR, Raman, calculated wave numbers and vibrational assignments of 2-Methylidene -4-oxo-4-[(2, 4, 5-trichlorophenyl) amino] Butanoic acid.

S.No.	Experimental frequency		Calculated frequency				Vibrational Assignment (PED)
	IR	Raman	B3LYP/DGDZVP2		B3LYP/DGTZVP		
			Unscaled	Scaled	Unscaled	Scaled	
1	3381		3757	3380	3762	3386	νOH(98)
2	3279		3486	3280	3531	3283	νNH(98)
3	3060	3061	3271	3250	3269	3256	νCH(98)
4			3250	3181	3250	3188	νasCH2(96))
5	3014	3020	3235	3061	3234	3066	νCH(98)
6			3167	3015	3166	3016	$\nu_{as}CH_2$(96)
7			3155	2961	3157	2959	$\nu_{ss}CH_2$(97)
8	2959		3091	2923	3087	2925	$\nu_{ss}CH_2$(98)
9	1687	1680	1801	1685	1802	1687	νCO(58)+δCO(22)+δOH(13)
10	1672		1756	1672	1759	1673	νCO(59)+δCN(20)+δNH(15)
11	1629	1629	1690	1630	1695	1635	νCC(71)+δCH2(11)
12		1597	1628	1598	1628	1592	νCC(71)+δscissCH(11)
13	1587		1618	1587	1616	1588	δNH(69)+δCC(20)
14	1569	1563	1548	1570	1545	1566	νCC(67)+δNH(13)
15	1455		1497	1450	1491	1459	δscissCH2(78)
16	1395	1390	1488	1393	1486	1397	νCC(62)+δCH(21)+δNH(11)
17			1461	1377	1464	1384	$\delta scissCH_2$(82)
18			1390	1360	1390	1390	νCC(74)+δCCl(12)+νCN(10)
19	1314		1377	1315	1373	1317	νCO(67)+δOH(16)+νCC(10)
20			1327	1254	1373	1250	$\delta_{rock}CH_2$(76)+νCC(10)
21	1235		1320	1238	1329	1239	νCC(81)
22			1285	1218	1329	1214	νCC(67)+δNH(16)+$\delta_{rock}CH_2$(10)
23			1271	1261	1319	1206	δCH(68)
24			1264	1180	1319	1185	δCH(72)+δOH(12)
25			1247	1160	1285	1163	δOH(76)+δCH(10)
26	1141		1178	1141	1269	1146	Ringδ(58)+δCH(27)
27		1132	1153	1130	1262	1133	δrockCH2(79)+νCO(10)
28		1100	1131	1102	1248	1104	τCH2(66)
29	1078		1079	1075	1174	1079	νCC(62)+$\gamma_{wagg}CH_2$(18))
30	960	966	980	962	1152	966	γCC(60)+δCH(16)+δCO(10)
31	918		972	920	1129	920	$\gamma_{wagg.}CH_2$(88)
32			962	902	1079	902	$\gamma_{wagg.}CH_2$(86)
33	877	875	947	877	982	879	νCC(60)+δCO(21)+νNH(10)
34	834		927	836	976	830	νCN(62)+δNH(17)+δCN(12)
35	821	820	916	821	954	826	γCH(89)
36	795		872	796	951	798	γCH(88)
37	750	750	833	751	925	753	γOH(52)+γCO(20)+γCC(12)
38	734		813	736	915	735	γCN(60)+γCO(20)+δCN(18)
39	725		798	726	872	726	γCCl(51)+γCC(27)+δOH(18)
40		680	743	681	743	682	γCCl(61)+δ_{Ring}(21)
41	672		715	670	708	677	γNH(77)
42			708	661	693	663	δ_{Ring}(70)+δCN(18)
43			687	643	676	635	νCCl(81)
44	624	625	666	625	644	625	τCH2(81)
45	561		635	567	631	566	δCCl(66)
46	543		606	540	613	545	δ_{Ring} (70)+δCN(18)
47		525	586	525	577	526	δCN(66)+δCO(18)
48			552	496	540	496	δCN(65)+δCO(18)+δCC(10)
49			534	470	517	472	δCN(65)+δCO(18)+δCC(10)

50			522	429	499	439	δCC(51)+δCH(28)
51			508	410	485	412	δCO(57)+δCCC(18)+νCC(10)
52			454	406	458	406	δCC(50)+δCO(19)
53		396	451	396	452	395	δCC(52)+δCO(20)
54			382	360	413	357	δCC(50)+δCO(19)
55		332	376	333	381	335	δCO(51)+δCC(21)+νCC(12)
56			349	317	371	316	δCO(52)+δCC(19)+γCC(10)
57		288	331	285	332	288	δ_{Ring} (66)+δCN(21)
58			302	262	315	266	δCC(57)+δCH2(20)
59		251	273	250	273	252	γCN(55)+γCC(21)+γCH(10)
60			261	230	249	231	γCC(53)+γCH2(18)
61		194	246	196	239	195	δCN(53)+νCC(20)+νCH(10)
62			201	182	195	180	νCCl(64)+δCN(17)+δCC(10)
63			193	155	191	163	δCCl(63)+δCN(16)+δCC(10)
64		142	171	140	170	145	γCC(60)+γCO(18)
65			125	110	126	112	γ_{Ring} (51)
66			113	91	111	89	γCCl(50)+γCN(19)+γCC(12)
67		77	96	76	87	78	γ_{Ring} (52)
68			71	60	64	61	γCCl(55)+γNH(19)+γ_{wagg}.CH2(12)
69			59	50	50	48	γC0(49)+γCC(23)+$\gamma_{wagg.}CH_2$(10)
70			51	39	38	35	γCCl(53)+γNH(19)+ $\gamma_{wagg.}CH_2$(12)
71		25	32	33	26	30	γCO(50)+γNH(21)
72			17	13	13	12	γCO(52)+γCN(23)+γCC(13)

ν –stretching, ν_{as} -asymmetric stretching, δ–in- plane bending, γ –out- of- plane bending,
τ -twisting, ρ - rocking, δrock – rocking δsciss- scissoring, δwag-wagging

In the present study, the band around 1395 and 1360 cm^{-1} are assigned to CH_2 scissoring modes which good agreement with the result 1435 cm^{-1} (FT-Raman) and 1427 cm^{-1} (FT-IR) for triazole thione by Roseline Sebastein et al.[18] and also reported that stretching modes of the same compound were appeared at 3115, 3113 and 3036 cm^{-1}. In line with his observation the weak IR band observed at 3060 cm^{-1} and the strong Raman band at 3061 cm^{-1} are assigned to the asymmetric stretching mode of the CH_2 group. The medium strong IR band observed at 2921 cm^{-1} and the weak Raman band at 2922 cm^{-1} are attributed to the symmetric stretching mode. Alaman et al. [19] reported that the CH_2 twisting frequency observed in the range 1180-1390 cm^{-1} of Carbonitrile compound. In the present study, the band around 1235 and 1216 cm^{-1} are assigned to CH_2 twisting. The wagging, and rocking modes of the CH_2 group are observed and lie within the expected range. Mary et al. [20] assigned that CH in-plane bending and out-of-plane bending vibrations are usually observed in the range 1000-1400 cm^{-1} and 520-970 cm^{-1}.

In present case, the CH in-plane bending vibrational frequencies are assigned at 1395, 1360, 1314 and 1183 cm^{-1} (IR spectrum) CH out-of-plane bending vibrational frequencies is assigned at 960, 918, 877 and 834 cm^{-1} (IR spectrum). The scissoring vibrations of the CH_2 group give bands in IR and Raman at 1395 and 1390 cm^{-1}. The CH_2 wagging vibration is found Raman bands at 1254 cm^{-1} and IR band at 1216 cm^{-1} are assigned to CH_2 wagging mode.

The identification of C-N vibration is very difficult task. Since mixing of several vibrations are possible in this region. Subashchandrabose et al. [21] assigned C-N stretching at 1476 cm^{-1} and 1294 cm^{-1} for bis (4-amino-5-mercapto-1,2,4-triazol-3-yl) methane. In the present study, the C-N stretching vibration are found to be observed at 1455 cm^{-1}, the corresponding Raman band is identified at 1428 cm^{-1}. The DFT computation predicts this vibrational mode at 1329 cm^{-1}. The C-N out-of-plane bending is assigned to a weak FT-Raman band at 332 cm^{-1} and 288 cm^{-1} shows a good agreement with the expected value. According to the literature [22, 23], the NH vibrations are expected in the following regions; stretching mode: 3500-3300 cm^{-1} and deformation modes: around 1500, 1250 and 750-600 cm^{-1}. For MTA, the NH stretching modes are assigned at 3279 cm^{-1} in the IR spectrum, 3213 cm^{-1} in the Raman spectrum and at 3531 cm^{-1} theoretically and NH deformations are assigned at 1329 cm^{-1} theoretically and experimentally bands are observed at 1285 cm^{-1} in the Raman spectrum and 1455 cm^{-1} at IR spectrum.

Carboxyl group is a functional group which can be most easily identified by IR spectroscopy. It is well known that the deprotonated carboxyl group COO^- has two important characteristic absorption bands: asymmetric stretching in the region 1650-1550 cm^{-1} and symmetric stretching near 1400 cm^{-1} [24]. In the present study, the vibration is observed at 1569 cm^{-1} in FT-IR spectrum and FT-Raman bands at 1597 cm^{-1} are assigned to C-O stretching mode. Similarly O-H in-plane bending vibrations are also identified at 3183 cm^{-1} in FT-IR and 3070 cm^{-1} at FT-Raman spectrum respectively. Edwin et al. [25] reported that the O-H stretching mode of the carboxylic group appears as a strong and broad peak in IR spectrum in the 2400-3400 cm^{-1} range. According to literature C=O stretching modes are expected in the region 1850-1550 cm^{-1}, and the C-O-C stretching modes are in the region 1200-900 cm^{-1} [26,27]. The C=O stretching modes of MTA are observed at 1681 cm^{-1} in the Raman spectrum and 1672 cm^{-1} at IR spectrum. The C-O-C stretching modes are assigned at 960 cm^{-1} in IR spectrum and at 967 cm^{-1} in Raman spectrum.

3.3 Mulliken charges

The calculation of atomic charges plays an important role in the application of quantum mechanical calculations to molecular systems [28]. Mulliken charges are calculated by determining the electron population of each atom as defined in the basic functions.

Mulliken charges analysis plots originated by calculations with the basis set B3LYP/DGDZVP2/DGTZVP are shown in Fig. 4 and Table 3. The total charge of the investigated complex is equal to zero. It is clearly shown that in both method, the atomic charge of carbon atoms attached to hydrogen are negative (C_6, C_3, C_{16} and C_{20}), while other remaining carbons which are connected to Oxygen, Carbon and Nitrogen have positive charge (C_1, C_{14} and C_{23}).

In MTA, C1 is attached to more electronegative nitrogen atom and hence have the most positive value while the most negative charge belongs to C20 atom, which is attached to double bonded C19 atom. All the hydrogen atoms have positive charges.

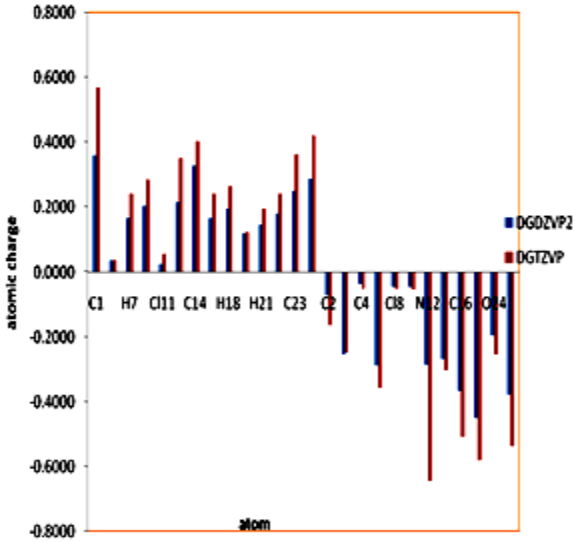

Fig 4. Mulliken atomic charges for 2-Methylidene -4-oxo-4-[(2, 4, 5-trichlorophenyl) amino] Butanoic acid.

Table 3. Mulliken charges of 2-Methylidene -4-oxo-4-[(2, 4, 5-trichlorophenyl) amino] Butanoic acid determined by DFT method at B3LYP/DGDZVP2 and DGTZVP level:

Positive charge			Negative charge		
Atoms	**DGDZVP2**	**DGTZVP**	**Atoms**	**DGDZVP2**	**DGTZVP**
C_1	0.3695	0.5697	C_2	-0.0705	-0.1647
C_5	0.0357	0.0373	C_3	-0.2533	-0.2460
H_7	0.1653	0.2422	C_4	-0.0371	-0.0503
H_{10}	0.2027	0.2839	C_6	-0.2874	-0.3575
Cl_{11}	0.0240	0.0551	Cl_8	-0.0436	-0.0521
H_{13}	0.2141	0.3522	Cl_9	-0.0456	-0.0526
C_{14}	0.3290	0.4047	N_{12}	-0.2854	-0.6444
H_{17}	0.1672	0.2418	O_{15}	-0.2685	-0.3021
H_{18}	0.1949	0.2653	C_{16}	-0.3654	-0.5085
C_{19}	0.1209	0.1218	C_{20}	-0.4496	-0.5807
H_{21}	0.1464	0.1943	O_{24}	-0.1957	-0.2537
H_{22}	0.1814	0.2421	O_{25}	-0.3775	-0.5379
C_{23}	0.2507	0.3628			
H_{26}	0.2868	0.4217			

3.4 Frontier molecular orbitals

Knowledge of the highest occupied molecular orbital (HOMO) and lowest unoccupied molecular orbital (LUMO) and their properties such as their energy is very useful to gauge the chemical reactivity of the molecule. The ability of the molecule to donate an electron is associated with the HOMO and the characteristic of the LUMO is associated with the molecule's electron affinity. The HOMO and LUMO energies are very useful for physicist and chemists are very important terms in quantum chemistry [29]. In the present study, the HOMO and LUMO energies have been predicted at B3LYP method with DGDZVP2 basis set. According to the calculated results, the energy value of HOMO is computed 4.617eV and the energy of LUMO is 2.125eV. As a result, a very small energy gap is observed between HOMO and LUMO is 2.419 eV. The distribution and energy levels of HOMO-LUMO orbital of MTA is shown in Fig. 5 and Table 4. The positive phase is red and the negative one is green.

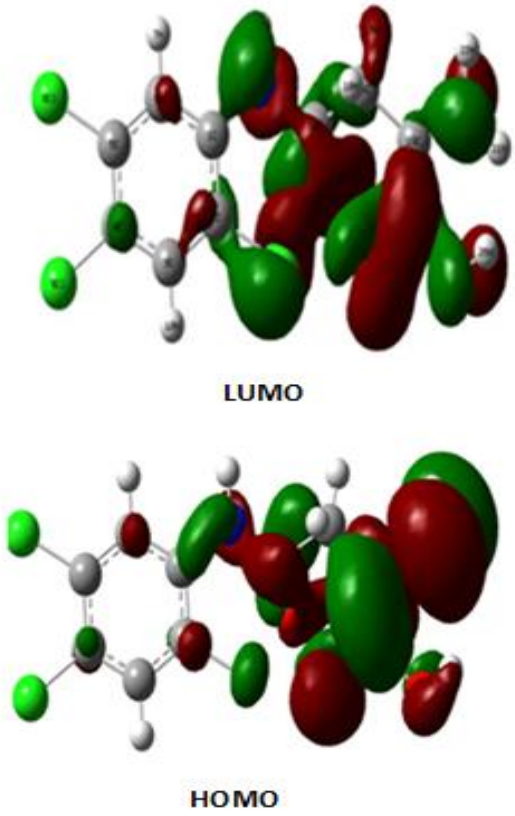

Fig 5. HOMO and LUMO plots of 2-Methylidene -4-oxo-4-[(2, 4, 5-trichlorophenyl) amino] Butanoic acid.

The chemical hardness and softness of a molecule is a good standard to value the chemical stability of a molecule. The chemical hardness and softness of a molecule depends on the energy gap between HOMO-LUMO. The molecules having a small energy gap are known as soft molecules and molecules having large energy gap are known as hard molecules. The soft molecules are more polarizable than the hard ones due to them need small energy to excitation. MTA have small energy gap, hence from the calculation we concluded that the molecule taken for investigation belongs to soft material. The lowering of the HOMO-LUMO band gap is essentially a consequence of the large stabilization of the LUMO due to the strong electron accepting ability of the electron acceptor group [30]. The energies of HOMO and LUMO and their neighbouring orbitals are all negative values, which indicate MTA is stable [31].

3.5 NBO analysis

NBO analysis has been performed on MTA at the B3LYP/DGDZVP2 level of theory in order to elucidate the intra-molecular, rehybridization and delocalization of electron density within the molecule. NBO analysis is proved to be an effective tool for chemical interpretation of hyper conjucative interaction and electron density transfer (EDT) from the filled lone electron pair of the n(y) of the "Lewis base" y into the unfilled anti-bond σ*(X….H) of the "Lewis acid" X…..H…..X in X……H…..Y hydrogen bonding systems [32]. The larger E (2) value, the more intensive is the interaction between electron donors and electron acceptors i.e. the more donating tendency from the electron donors to electron acceptors and the greater extend of conjugation of the whole system. The hyper conjugative interaction energy was deduced from the second order perturbation approach [33].

Table 4. HOMO and LUMO energies gap values (eV) and related molecular properties of 2-Methylidene -4-oxo-4-[(2, 4, 5-trichlorophenyl) amino] Butanoic acid based on B3LYP/LANL2DZ method.

Molecular Properties	Energy (eV)	Energy gap (eV)	Ionization potential (I)	Electron affinity (A)	Global hardness (η)	Electro negativity (χ)	Chemical softness (σ)	Chemical potential (μ)	Global Electrophilicity (ω)
E_{HOMO}	4.617	2.492	0.21934	0.08471	0.06731	0.05332	14.85552	-0.05332	0.21117
E_{LUMO}	2.125								
E_{HOMO-1}	3.404	2.600	0.22747	0.04093	0.09327	0.1342	10.72156	-0.13420	0.0651
E_{LUMO+1}	0.804								
E_{HOMO-2}	2.568	2.8	0.2862	0.00957	0.13831	0.14788	7.23013	-0.14788	0.07902
E_{LUMO+2}	0.232								

The high values of polarization coefficient, show the large electron density i.e. igh electro negativity are found for σ (C_2-Cl_{11}), σ(C_{12}-C_{14}), σ(C_{14}-O_{15}) and σ(C_{23}-O_{24}) bonding (Table 5). The large E (2) values i.e. intensive interaction are found for σ(C_1-C_2)→ σ*(C_3-C_4), σ(C_1-C_2)→ σ*(C_5-C_6), σ(C_3-C_4)→ σ*(C_1-C_2), σ(C_3-C_4)→ σ*(C_5-C_6), σ(C_5-C_6)→ σ*(C_1-C_2), σ(C_5-C_6)→σ*(C_3-C_4), LPN_{12}→σ (C_1-C_2), LPN_{12}→π(C_{14}-O_{15}), LPO_{24}→ σ(C_{14}-O_{15}), LPO_{25}→π(C_{23}-O_{24}).

The electron population computations are important because theseare related to electronic structure, dipole moment , polarizability, chemical reactivity and other properties of molecule. In Table 6, BD (C_{23}-O_{24}) orbital with 1.9884 a.u energy has 68.5% of C_{23} character in a $sp^{2.04}$ hybrid and has 31.5% O_{24} character in a $sp^{1.88}$ hybrid. The idealized sp^2 hybrid has 75% p-character. The two coefficients 0.8277and 0.5612 are called polarization coefficients. The sizes of these coefficients show the importance of the two hybrids in the formation of the bond. The oxygen (O_{15}) has larger percentage of this NBO, 68.94% and gives the larger polarization coefficient 0.8303 because it has the higher electronegativity. Similarly, BD (C_1-C_2), BD (C_1-C_6), BD (C_1-N_{12}) and BD (C_2-Cl_{11}) bonding orbital also show that carbon and nitrogen have the lesser percentage of NBO and give the lesser polarization coefficient as compared BD (C_{23}-O_{24}) bond.

Table 5.Important donor – acceptor interaction based on second order perturbation theory analysis of Fock matrix in NBO basis.

Donor(i)	Type	ED(i)/e	Acceptor(j)	Type	ED(j)/e	E(2)(KJ/mol)
C_1-C_2	σ	0.3	C_3-C_4	σ	0.078	24.78
C_3-C_4	σ	0.29	C_5-C_6	σ	0.076	23.33
C_1-C_2	σ	0.3	C_5-C_6	σ	0.071	20.38
C_5-C_6	σ	0.31	C_1-C_2	σ	0.075	21.11
C_5-C_6	σ	0.31	C_3-C_4	σ	0.07	18.85
C_{19}-C_{20}	σ	0.28	C_{23}-O_{24}	σ	0.062	15.24
C_{14}-O_{15}	σ	0.36	C_{23}-O_{24}	σ	0.068	13.87
C_3-H_{10}	π	1.08	C_1-C_2	π	0.073	6.13
C_3-H_{10}	π	1.07	C_4-C_5	π	0.073	6.21
C_6-H_7	π	1.08	C_1-C_2	π	0.074	6.29
C_6-H_7	π	1.07	C_4-C_5	π	0.072	6.05
C_{16}-H_{18}	π	0.51	C_{14}-O_{15}	π	0.054	6.1
C_{20}-H_{21}	π	0.92	C_{16}-C_{19}	π	0.074	7.43
C_{20}-H_{22}	π	0.92	C_{19}-C_{23}	π	0.075	6.1
$LP(2)O_{24}$	σ	0.35	C_{14} - O_{15}	σ	0.1	29.84
$LP(2)O_{25}$	σ	0.36	C_{23} - O_{24}	σ	0.1	31.26
$LP(1)N_{12}$	π	0.29	C_1 - C_2	σ	0.09	28.71
$LP(1)N_{12}$	π	0.25	C_{14} - O_{15}	σ	0.08	28.66

E(2) – mean energy of hyper conjugative interactions.

E(j) – E(i) – energy difference between donor and acceptor i and j NBO orbital's

3.6 Molecular electrostatic potential

The MEP is a plot of electrostatic potential mapped onto the constant electron density surface. It is very useful in research of molecular structure with its physiochemical property relationship as well as hydrogen bonding interactions [34]. This is also provides information for understanding the shape, size, charge density, delocalization and site of chemical reactivity of the molecule. To investigate the reactive sites of MTA, the molecular electrostatic potential surface (Fig. 6) was plotted. In the molecular electrostatic potential map, different colors are used to represent the different values of the electrostatic potentials; most electronegative regions by red, most positive electrostatic potential by blue and zero potential by green. Potential increases in the order red>orange>yellow>green>blue. The red color surfaces with negative MEP belong to high electron density, indicating a strong attraction between the proton and points on the molecular surface. The blue color surfaces correspond to areas of lowest electron density. In MEP map, the surfaces over the oxygen atoms representing maximum negative electrostatic potential and the surfaces over the Hydrogen with maximum positive electrostatic potential may be site of electrophilic and nucleophilic reactions, respectively. From these results, we can say that the O_8 and H_9 indicate the strongest attraction and O_{10} atom indicate strongest repulsion. As can be seen from the Fig. 6 the negative electrostatic potential regions are mainly localized of carbonyl group and are possible sites for electrophilc attack. The positive regions are localized all the rings, indicating possible sites for nucleophilic attack. The knowledge of the molecular reactive site enables workers to predict how complex drugs interact with proteins.

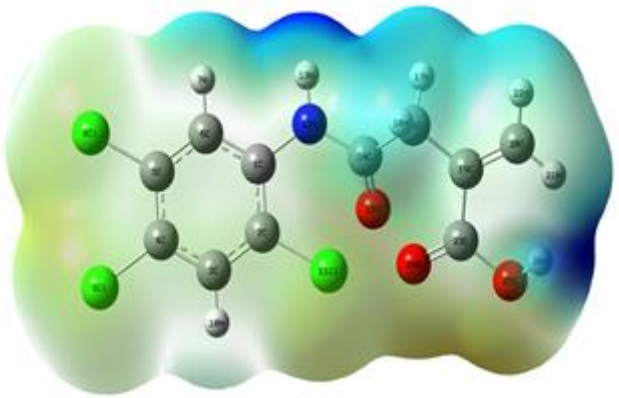

Fig 6.Molecular electrostatic potential map for 2-Methylidene -4-oxo-4-[(2, 4, 5-trichlorophenyl) amino] Butanoic acid.

3.7 NMR analysis

Nuclear magnetic resonance (NMR) spectroscopy has become a valuable screening tool for the binding of ligands to protein targets, and has the key advantage of being able to detect and quantify interaction with high sensitivity without requiring prior knowledge of protein function. The experimental ^1H and ^{13}C NMR spectra of MTA are shown in Fig. 7 and 8. The computed ^1H NMR chemical shifts at the B3LYP/DGDZVP2 levels of theory along with experimental data are given in Table 7. As can be seen, the results obtained by using DFT/B3LYP/DGDZVP2 method are in better agreement with experimental data. It can be seen from the Table 7, the ^{13}C chemical shifts are >100, which ensures the molecules to be organic [35-37].

Table 6. NBO analysis for selected bonding and lone pairs in 2-Methylidene -4-oxo-4-[(2, 4, 5-trichlorophenyl) amino] Butanoic acid.

Bond(A-B)	Type	ED/energy(a.u)	ED (A%)	ED (B %)	NBO	S%	P%
Cl_8	σ	1.988-0.022			$sp^{0.23}$	81.15	18.83
Cl_{11}	σ	1.973-.00784			$sp^{0.53}$	65.14	34.84
Cl_9	σ	1.988.00272			$sp^{0.23}$	81.19	18.79
O_{15}	σ	1.951-0.00897			$sp^{0.97}$	50.73	49.17
O_{24}	σ	1.9448-0.005			$sp^{0.86}$	53.76	46.21
O_{25}	σ	1.9760.002			$sp^{1.06}$	48.47	51.46
C_1-C_2	σ	1.9707-0.041	50.46	49.54	$0.7103(sp^{1.71})$ $+0.7038(sp^{1.64})$	36.83 37.82	63.11 62.12
C_1-C_6	σ	1.96077-0.02178	50.55	49.45	$0.711(sp^{1.70})$ $+0.7032(sp^{1.77})$	37.07 36.11	62.89 63.83
C_1-N_{12}	σ	1.9773-0.0364	37.99	62.01	$0.6163(sp^{2.86})$ $+0.7875(sp^{1.83})$	25.9 35.37	73.99 64.59
C_2-Cl_{11}	σ	1.968-0.06775	46.07	53.93	$0.6788(sp^{3.21})$ $+0.7344(sp^{5.95})$	23.72 14.32	76.1 85.2
N_{12}-C_{14}	σ	1.9807-0.08019	63.93	36.07	$0.7995(sp^{1.91})$ $+0.6006(sp^{2.30})$	34.36 30.24	65.6 69.6
C_{14}-O_{15}	σ	1.9889-0.345	31.06	68.94	$0.5574(sp^{2.29})$ $+0.8303(sp^{1.68})$	30.34 37.23	69.46 62.5
C_{23}-O_{24}	σ	1.9884-0.3355	31.5	68.5	$0.5612(sp^{2.04})$ $+0.8277(sp^{1.88})$	32.79 34.64	66.94 65.28
C_1-C_2	π	1.9707-0.0228	49.54	50.46	$0.7038(sp^{1.71})$ $-0.7103(sp^{1.64})$	36.83 37.82	63.11 62.12
C_1-C_6	π	1.96077-0.0217	49.45	5055	$0.703(sp^{1.70})$ $-0.711(sp^{1.77})$	37.03 36.11	62.89 63.83
C_1-N_{12}	π	1.9773-0.03648	62.01	37.99	$0.7875(sp^{2.86})$ $-0.6163(sp^{1.83})$	25.9 35.37	73.99 64.59
C_2-Cl_{11}	π	1.968-0.06775	53.93	46.07	$0.7344(sp^{3.21})$ $-0.6788(sp^{5.95})$	23.72 14.32	76.1 85.2
N_{12}-C_{14}	π	1.980-0.08019	36.07	63.93	$0.6006(sp^{1.91})$ $-0.7995(sp^{2.30})$	34.36 30.24	65.6 69.6
C_{14}-O_{15}	π	1.988-0.34507	64.79	35.21	$0.8049(sp^{61.28})$ $-0.5934(sp^{99.99})$	1.6 0.86	98.28 98.89
C_{23}-O_{24}	π	1.8977-0.03603	68.5	31.5	$0.8277(sp^{2.04})$ $-0.5612(sp^{1.88})$	32.79 34.64	66.94 65.28

The proton NMR signals have been observed in between 1.0 and13.0 ppm while carbon NMR signals are found in between 100 and 172 ppm. The observed experimental chemical shift positions of ring carbon atoms lie in the range 125.817-169.891 ppm. The highest chemical shifts of C_{23}, C_{14} and C_{19} are 172.43, 169.89 and 168.04 ppm respectively, which shows the bonding with electron attracting species (oxygen). The experimental chemical shift of proton attached to oxygen is observed at 6.97 ppm. This shift to low field indicates intra-molecular hydrogen bonding between O_{25}-H_{26}.

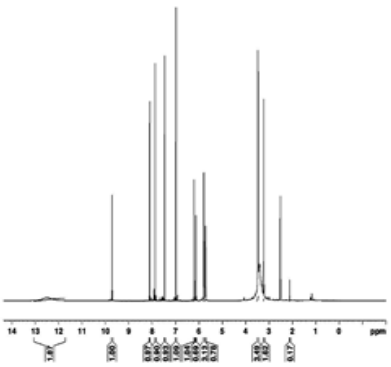

Fig 7. ^{1}H spectrum of 2-Methylidene -4-oxo-4-[(2, 4, 5-trichlorophenyl) amino] Butanoic acid.

The signal at 7.465 ppm is assigned to proton attached to nitrogen. Aromatic Protons H_7 and H_{10} have these values 8.1 and 9.7 ppm.

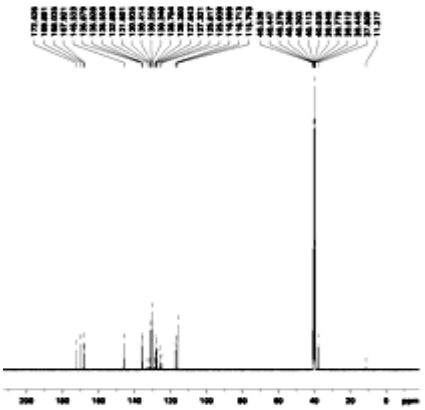

Fig 8. ^{13}C spectrum of 2-Methylidene -4-oxo-4-[(2, 4, 5-trichlorophenyl) amino] Butanoic acid.

3.8 Non linear optical properties

The computational approach allows the determination of molecular NLO properties as an inexpensive way to design molecules by analyzing their potential before synthesis and to determine high-order hyper polarizability tensors of molecules.

The dipole moment and dipole polarizability are properties of universal importance for molecular science [38]. The density functional theory has been used to calculate the dipole moment (μ), mean polarizability (α), and the total first static hyper polarizability (β) in terms of x,y,z components and are given by following equations [39].

$\mu = (\mu_x^2+\mu_y^2+\mu_z^2)^{1/2}$

$\mu_\alpha = 1/3(\alpha_{xx}+\alpha_{yy}+\alpha_{zz})$

$\beta_{tot} = (\beta_{xxx}+\beta_{xyy}+\beta_{xzz})^{1/2}+(\beta_{yyy}+\beta_{yzz}+\beta_{yxx})^{1/2}+(\beta_{zzz}+\beta_{zyy}+\beta_{zxx})^{1/2}$

The polarizability and hyper polarizability tensors (α_{xx}, α_{yy}, α_{zz}, β_{xxx}, β_{xyy}, β_{yzz}, β_{yxx}, β_{zzz}, β_{zyy}, and β_{zxx}) can be obtained by a frequency job output file of Gaussian. However, α and β values of Gaussian output are in atomic units (a.u), so they have been converted into electrostatic units (e.s.u). The first order hyper polarizability of MTA is calculated and is found to be 12.28x10-30 e.s.u. The calculated hyper polarizability of MTA is greater than of the standard NLO material Urea (0.13x10-30 e.s.u) [40]. The high value of dipole moment and first order hyperpolarizability reflect the non-linear property of MTA. The amount of charge transferred for the molecule. Increase of π-conjugated chain length in organic molecules, in general, enhances the magnitude of hyperpolarizability, depends on the nature of the end group of the molecule. From the Table 8, the large β value calculated by the B3LYP method shows that the studied compound is a good NLO material and is suitable for further non linear optical studies.

Table 7. Comparison of calculated ^{1}H NMR and ^{13}C NMR chemical shifts (ppm) with experimental values for 2-Methylidene -4-oxo-4-[(2, 4, 5- trichlorophenyl) amino] Butanoic acid.

Atom	Exp.	B3LYP/ DGDZVP2	Proton (multiplicity)	Exp.	B3LYP/ DGDZVP2
C_1	125.82	125.94	H_{10}(s)	9.71	9.01
C_2	145.53	158.02	H_7(s)	8.1	8.64
C_3	130.26	130.65	H_{13}(s)	7.46	7.77
C_4	135.83	135.87	H_{26}(s)	6.97	6.91
C_5	116.71	116.52	H_{22}(d)	6.19	6.68
C_6	115.76	114.89	H_{21}(t)	5.78	5.68
C_{14}	169.89	169.35	H_{17}(s)	3.46	3.64
C_{16}	37.81	39.745	H_{18}(t)	2.51	2.3
C_{19}	168.04	168.36			
C_{20}	40.54	40.332			
C_{23}	172.43	168			

s-siglet, d-doublet and t-triplet

Table 8.Electric dipole moment μ(debye), mean olarizability α_{tot}(e.s.u.), anisotropy polarizability $\Delta\alpha$(e.s.u.) and first order hyperpolarizability β_{tot}(×10-30 e.s.u.) for 2-Methylidene -4-oxo-4-[(2, 4, 5-trichlorophenyl) amino] Butanoic acid at B3LYP/ZVP2 and B3LYP/DGTZVP methods.

Parameters	B3LYP/ DGDZVP2	Parameters	B3LYP/ DGDZVP2	Parameters	B3LYP/ DGDZVP2
μ_x	4.4230	α_{yy}	3.7352	β_{xxy}	36.1561
μ_y	5.5875	α_{yz}	-1.4451	β_{xxz}	42.5547
μ_z	1.8433	α_{zz}	-128.3088	β_{xzz}	1.3496
μ	7.3607	β_{xxx}	208.6603	β_{yzz}	-4.5918
α_{xx}	-117.2511	β_{yyy}	27.3758	β_{yyz}	-1.3491
α_{xy}	12.4586	β_{zzz}	-4.4302	β_{xyz}	-1.389642
α_{xz}	9.6388	β_{xyy}	-3.5211	β_{tot}	3.8145×10^{-30}

3.9 Local reactivity descriptors

Fukui functions play a prominent role in the field known as conceptual Density functional theory (DFT). Based on the original ideas of Fukui; they are introduced as quantities that reflect the response of a molecular system towards a change in the number of electrons (Ne) of the molecular system under consideration [41]. They were introduced as a local quantity, which is depending on the spatial coordinates. The most relevant local descriptor of reactivity is the Fukui function. The Fukui function indicates the propensity of the electronic density to deform at a given position upon accepting or donating electrons [42-44]. The Fukui function is a function defined at each point of space, but it is useful to define a condensed Fukui function. In this case, Fukui functions are condensed to an atom, as defined by a partition scheme. The condensed forms of Fukui functions for an atom k in a molecule are expressed as:

$f_k^+ = q_k(N+1) - q_k(N)$, for a nucleophilic attack

$f_k^- = q_k(N) - q_k(N-1)$, for an electrophilic attack

$f_k^0 = 1/2\{q_k(N+1) - q_k(N-1)\}$ for a hemolytic attack

where q_k is the atomic charge (evaluated from Mulliken population analysis) at the k^{th} atomic site in the neutral (N), anionic (N+1) or cationic (N -1) chemical species. Morell et al. [45] recently proposed a dual descriptor Δf(r), which is defined as the difference between the nucleophilic and electrophilic Fukui function and is given by,

$\Delta f(r) = [f^+(r) - f^-(r)]$

Δf(r)<0, then the site is favoured for an electrophilic attack, whereas Δf(r)>0, then the site may be favoured for a nucleophilic attack. Under this situation, dual descriptors Δf(r) provide a clear difference between nucleophilic and electrophilic attack at a particular site with their sign. From Table 9, according to the condition for dual descriptor, nucleophilic sites for in our title compound are C_5, H_7, C_{18}, C_{19}, H_{10}, Cl_{11}, N_{12}, H_{13}, O_{15}, C_{16}, H_{17}, C_{23}, O_{24}, O_{25}, H_{26} (positive values i.e Δf(r)>0). Similarly the electrophilic attack sites are C_1, C_2, C_3, C_4, C_6, C_{14}, H_{18}, C_{19}, C_{20}, H_{21}, H_{22} (negative values i.e Δf(r) <0).

3.10 Molecular Docking

PASS (prediction of activity spectra) [46] is an online tool which predicts different types of activities based on the structure of a compound. Molecular docking is an efficient tool to get an insight into ligand-receptor interactions and screen molecules for the binding affinities against a particular receptor. All molecular docking calculations were performed on Auto Dock-vina software [47]. The 3D structure of Beta-lactamase Oxa-58 was obtained from protein data bank (PDB ID: 4Z9Q) [48]. 2-Methylidene -4-oxo-4-[(2, 4, 5-trichlorophenyl) amino] Butanoic acid structure was created by using "Chemdraw". The Auto Dock tools graphical user interface was used to calculate Geisteger charges, add polar hydrogen and partial charges using Kollman united charges. The active site of the enzyme was defined to include residues of the active site within the grid size of 60Å x 60Å x 60Å. The most popular algorithm, Lamarckian Genetic Algorithm (LGA) available in AutoDock was employed for docking [49, 50]. PASS prediction activity spectrum of the title compound is given in Table (Table 10) and docking protocol was tested by docking the co-crystallized inhibitor onto the enzyme catalytic site which showed perfect energy within the co-crystallized ligand with RMSD [51] well within the allowed range of 2Å [52]. The present study helps us to understand the interaction between the title compound and receptor Beta-lactamase Oxa-58 and also explore their binding mode (Fig 9, 10). The calculated binding energy value is 6.7Kcal/mol.

Table 9. Calculated Fukui functions of 2-Methylidene -4-oxo-4-[(2, 4, 5-trichlorophenyl) amino] Butanoic acid.

Atoms	fi^+	fj^-	fj^0	Δf^0	Atoms	fi^+	fj^-	fj^0	Δf^0
C_1	-0.0215	-0.0203	-0.0209	-0.0012	C_{14}	-0.0723	-0.0331	-0.0527	-0.0392
C_2	-0.0377	-0.0374	-0.0376	-0.0003	O_{15}	-0.0170	-0.0832	-0.0501	0.0661
C_3	0.0009	0.0059	0.0034	-0.0049	C_{16}	-0.0167	-0.0182	-0.0174	0.0015
C_4	-0.0379	-0.0302	-0.0340	-0.0077	H_{17}	-0.0419	-0.0463	-0.0441	0.0044
C_5	-0.0127	-0.0153	-0.0140	0.0026	H_{18}	-0.0421	-0.0410	-0.0416	-0.0011
C_6	-0.0284	-0.0238	-0.0261	-0.0046	C_{19}	-0.0170	0.0257	0.0044	-0.0427
H_7	-0.0218	-0.0228	-0.0223	0.0010	C_{20}	-0.1953	-0.1204	-0.1579	-0.0748
Cl_8	-0.0302	-0.0312	-0.0307	0.0010	H_{21}	-0.0366	-0.0233	-0.0300	-0.0133
Cl_9	-0.0283	-0.0296	-0.0290	0.0013	H_{22}	-0.0427	-0.0386	-0.0406	-0.0041
H_{10}	-0.0498	-0.0499	-0.0498	0.0001	C_{23}	-0.0695	-0.0820	-0.0758	0.0125
Cl_{11}	-0.0084	-0.0309	-0.0197	0.0225	O_{24}	-0.0646	-0.0770	-0.0708	0.0124
N_{12}	0.0072	-0.0170	-0.0049	0.0242	O_{25}	-0.0540	-0.0701	-0.0621	0.0160
H_{13}	-0.0384	-0.0488	-0.0436	0.0103	H_{26}	-0.0232	-0.0411	-0.0322	0.0180

The ligands formed two hydrogen bonds with residues, LYS 162 and TYR 158 (Fig.11). On comparing binding pattern of the receptor with other butanoic acid, found that binding with active site in terms of hydrogen bonds with the various residues. Our docking results indicated that the said compound bound in the pocket include the residues construct the active pocket of Beta-lactamase Oxa-58.

Table 10.The binding energy value of 2-Methylidene -4-oxo-4-[(2, 4, 5-trichlorophenyl) amino] Butanoic acid compound predicted by Autodockvina.

Protein PDB ID	Bonded residues	No. of Hydrogen bond	Bond Distance Å	Estimated inhibition Constant (μM)	Binding energy (kcal/mol)	Reference RMSDÅ
4Z9Y	LYS 162 TYR 158	2	1.7 2.0	12.24	6.70	35.81

Table 11.PASS Prediction of activity spectrum, Pa is the probability of the molecular to be active and Pi is the probability to be inactive.

Pa	Pi	Activity
0.740	0.036	Gluconate 2 – dehydrogenase (Acceptor inhibitor
0.740	0.058	Phobic disorder treatment
0.656	0.003	Prostaglan E1 antagonist
0.643	0.006	Gestagn antagonist
0.614	0.023	C1 transporting ATPase inhibitor
0.594	0.026	Muramoyltetrapeptide carboxypeptidase inhibitor
0.568	0.007	Ophthalmic drug
0.562	0.005	Antinuoplastic (Servical cancer)
0.601	0.074	Acrocylindropepsin inhibitor
0.601	0.074	Chymosin inhibitor

4.0 Conclusion

FT-IR and FT-Raman spectra of the 2-Methylidene -4-oxo-4-[(2, 4, 5-trichlorophenyl) amino] Butanoic acid were recorded and studied experimentally and theoretically. The details interpretation of normal modes has been made on the basis of PED calculations. The difference in HOMO and LUMO energy supports the charge transfer interaction with in the molecules. MEP predicts the most reactive part in the molecule. The NLO is identified as a featured attribute of the title compound which was inspected and authenticated via computed polarizability and hyperpolarizability. The NBO analysis reproduced the presence of hydrogen bonding, intermolecular delocalization and hyperconjucation in the title compound.

The calculated ^1H and ^{13}C NMR results are in good agreement with experiment data. From docking study, we conclude that the compound in consideration may be an effective protein inhibitor if further biologic explorations are carried out.

References

[1] H.M. Hamer, D. Jonkers, K. Venema, S. Vanhoutvin, F.J. Troostand, R.J. Brummer, Ali ment. Pharmacol. Ther. 27 (2009) 104 - 119.
[2] Y. Cao. H.Q. Li., J. Zhang, Ind. Eng. Chem. Res. 50 (2011) 7808 - 7814.
[3] C. Zhang, H. Yang, F. Yang, Y. Ma, Curr. Microbiol. 59 (2009) 656 - 663.
[4] El. Shafee, G.R. Saad, S.M. Fahmy, Eur. Polym. J. 37 (2001) 2091 - 2104.
[5] D.W. Armstrong, H. Yamazaki, Trends in Bio technology 4 (1986) 264 - 267.
[6] C. Shu, J. Cai, L. Huang, X. Zhu, Z. Xu, J. Mol. Catal. B 72 (2011) 139 -144.
[7] V. Crupi, D. Majolino. M.R. Mondello, P. Migliardo, V. Venuti, Bio. Med. Ana. 29 (2002) 1149 - 1152.
[8] G. Fini, Infrared and Raman spectroscopy in forensic science, J. Raman spectrosc. 35 (2004) 335 - 337.
[9] M.J. Frisch, G.W. Trucks, H.B. Schlegal, G.E. Scuseria, M.A. Robb, J.R. Cheesm, G. Zakrzewski, J.A. Montgomerg, R.E. Stratmann, J.C. Burant, Sapprich, J.M. Milliam, A.D. Daniels, K.N. Kudin, M.C. Strain, O. Farkas, J. Tomasi, V. Barone, M. Cossi, R. Camme, B. Mennucci, C. Pomelli, C. Adamo, S. Clifford, J. Ochterski, G.A.Petersson, P.Y. Ayala, Q. Cui. K. Morokuma, N. Rega, P. Savador, J.J. Dannenberg, D.K. Malich, A.D. Rabuck, K. Raghavac hari, J.B. Foresman, J. Cioslowski, J.V. Ortiz, A.G. Baboul, B.B. Stetanov, G.Liu, A. Liashe ko, P. Piskorz, I. Komaromi, R. Gomperts, R.L. Martin, D.J. Fox, T. Keith, M. Al- Laham, C.Y. Peng, A. Nsnsyskkara, M. Challacombe, P,.M.W. Gill, B.Johnson, W. Chen, M.W. Wong, J.L. Andres, C. Gonzalez, M. Head- Gordon, E.S. Replogle, J.A. Pople, GAUSSIAN09, Revision 02, Gaussian. Inc. Pittsburg, PA, 2009.
[10] A.D. Becke, J. Chem. Phys. 98 (1993) 5648.
[11] C. Lee, W. Yang, R.G. Parr, Phys. Rev. 37 (1998) 785.
[12] H. Jamroz, Vibrational energy distribution analysis VEDA 4.0 program, Warsaw, 2004.
[13] M.J. Frisch, A.B. Nielson, A.J. Holder, Causs view Users Manual, Gaussian Inc. Pittsburgh, PA, 2000.
[14] Y. Sheena Mary, H. Varghese, C.Y. Panicker, T. Thiemann, A. AlSaadi Saheed, A. Popoola, C. Van Alsenoy, Y. Al Jasem, Spectrochim. Acta A 150 (2015) 533 - 542.

[15] Y. Erdogu, M. Tahir Gulluoolu, S. Yurdakul, J. Mol. Struct 889 (2009) 361 - 370.
[16] S. Guidara, A. Ben Ahmed, Y. Abid, H. Feki, Spectrochi m. Acta A 127 (2014) 275 - 285.
[17] V. Arjunan, P.S. Balamourougane, C.V. Mythili, S. Mohan, J. Mol. Struct. 1003 (2011) 92 - 102.
[18] S.H. Roseline Sebastein, S. R. Mohammed, I. Attia, S. Al mutairi, A. El-Emam,Y. Painicker, C. Van Alenoy, Spectrochim. Acta A 132 (2014) 295 - 304.
[19] N. Z.Alaman, Y. Sheena Mary, C. Yohannan Panicker, I. Al-Swaidan, A. El-Emam, O. A. Al-Deeb, A. Abdulaiziz, A. Al-saadi, C.Van Alsenoy, J.Ahmad War, Spectrochim. Acta A 139(2015) 413 - 424.
[20] Y. Sheena Mary, Hema Tresa Varghese, C. Yohannan Panicker, M. Girisha, B.K. Sagar, H. Sathirajan, A. Alsaadi Saheed, C.Van Alsenoy, Spectrochim. Acta A 150 (2015) 543 - 545.
[21] S. Subashchandrabose, R. Krishnan, H. Saleem, R. Param eswari, N. Sundraganesan, V. Thanickachalam, G. Manickam, Spectrochim. Acta A 77 (2010) 877 - 884.
[22] N.B. Colthup, H. Daly, S.E. Wiberly, Academic press, Newyork, 1975.
[23] L.J. Bellamy, Third Edition, Chapman and Halls, Londan, 1975.
[24] N. Elleuch, A. Ben Ahmed, Y. Abid, H. Feki C. Minot, Spectrochim. Acta A 121 (2014) 129 - 138.
[25] B. Edwin, M. Amalanathan, I. Hubert Joe, Spectrochim. Acta A 96 (2012) 10 - 17.
[26] G. Socrates, John Wiley and sons, Newyork, 1981.
[27] J.B. Bhagyasree, J. Smuel, H.T. Varghese, C. Y. Panicker , M. Arisoy, O. Temiz, Spectro chim. Acta A 115 (2013) 79 - 91.
[28] S. Sebastian, K. Udayakumar, T. Jayavarthanan, N. Sund araganesan, Spectrochim. Acta A 96 (2012) 401 - 412.
[29] D .Shoba, S.Periandy, S. Boomadevi, S.Ramalingam, E. Fereduni, Spectrochim. Acta A 118 (2014)438-447.
[30] B. Edwin, M. Amalanathan, I. Hubert Joe, Spectrochim. Acta A 96 (2012) 10 - 17.
[31] R.N. Singh, A. Tiwari, P. Vikas Baboo, R.K. Divya Verma, Spectochim. Acta A 92 (2012) 295 - 304.
[32] T. Joselin Beacula, D. Manimaran, I. HubertJoe, V.K. Rastogi, V. Bena jothy, Spectrochim. Acta A 126 (2014) 170 - 177.
[33] D. M. Suresh, M. Amalanathan, V. Benajothy, Spectrochim. Acta A. 130 (2014) 591 - 603.
[34] O.A. ElGammal, T.H. Rakha, H.M. Metwally, G.M. Abu El-Reash, Spectrochim. Acta A 127 (2014) 144 - 156.
[35] H. shingh, S. Singh, A. Srivastava, P. Tandan, P. Bharti, S. Kumar, R. Maurya, Spectro chim. Acta A 120 (2014) 405 - 415.
[36] R. Dichfield, (1974) Mol.Phys.27, 789-807.
[37] C. Portela, M. Afonso, .M. Pinto, M.J. Ramos, 2003, FEBS Letters 27435.
[38] M. Amalanathan, T.S. Xavier, I. Hubert Joe, V.K. Rastog i, Spectrochim. Acta A 116 (2013) 574 - 583.
[39] I. Sheikhshoaie, S. Yousef, E. Sheikhshoaie, R. Mahdeyeh, H. Sheikhshoaie, H. Rudbari, Moj Khaleghi, Giuseppe Bruno, Spectrochim. Acta Part A 124 (2014) 548 - 555.
[40] M. Adant, L. Dupuis, L. Bredas, J. Quantum chem. 56 (2004) 497 - 507.
[41] P. Bultinck, R. Carbo Dorca, J. Math. Chem. 34 (2003) 1-2.
[42] R.G. Parr, W. Yang, Oxford University Press, New York, 1989.
[43] P.W. Ayers, R.G. Parr, J. Am. Chem. Soc. 122 (2000) 2010 - 2018.
[44] R.G. Parr, W.J. Yang, J. Am. Chem. Soc. 106 (1984) 4049 - 4050.
[45] C. Morell, A. Grand, A.T. Labbe, J. Phys. Chem. A 109 (2005) 205 - 212.
[46] S. parveen, A. Monirah, A. Alshaikh, C. Y. Panicker, A. El-Mustafa Arisoy, O.Temiz- Arpaci, C. Van Alsenoy, J. Mol. Struct. 1115 (2015) 94 - 104.
[47] A. Trott, J. Olson, J. Comput. Chem. 31 (2010) 455 - 461.
[48] http://www.resb.org/pdb/home/home.do
[49] G.M. Morris, D.S. Goodsell, R.S. Halliday, R. Huey, W.E. Hart, R.K. Belew, A.L. Olson, J. Comput. Chem.. 19 (1998) 1639 - 1662.
[50] R. Huey, G.M. Morris, A.L. Olson, D.S. Goodsell, J. Comput. Chem. 28 (2007) 1145 - 1152.
[51] Accelrys software Inc., Discovery studio Modeling environment, Release 4.0, san Diego, 2013.
[52] D.J. Kempf, K.C. Marsh, J.F. Denissen, E.Mc. Donald, S. Vasavanonda, C.A. Flento, B.E. Gren, L. Fino, C.H. Park, X.P. Kong, N.E. Wideburg, A. Saldivar, L. Ruiz, W.M. Kati, H.L. Sham, T. Robins, K.D. Stewart, A. Hsu, J. J. Platner, J.M. Leonard, D.W. Norbeck, Proc. Natl. Acad. Sci. USA 9 (1995) 2484 - 2488.